PCCP

PAPER

View Article Online
View Journal | View Issue

Cite this: *Phys. Chem. Chem. Phys.*, 2015, **17**, 25191

Combined experimental and computational NMR study of crystalline and amorphous zeolitic imidazolate frameworks†

Emma F. Baxter,[a] Thomas D. Bennett,[a] Caroline Mellot-Draznieks,[b] Christel Gervais,[c] Frédéric Blanc[d] and Anthony K. Cheetham*[a]

Received 1st May 2015,
Accepted 1st September 2015

DOI: 10.1039/c5cp02552d

www.rsc.org/pccp

Zeolitic imidazolate frameworks (ZIFs) have attracted great interest in recent years due to their high chemical and thermal stability with promising applications in gas storage and separations. We investigate the structures of three different crystalline ZIFs – ZIF-4, ZIF-8, ZIF-zni – and their amorphous counterparts using high field ^{13}C and ^{15}N CP MAS NMR. The high field (20 T) allows for the observation of all crystallographically independent carbon and nitrogen atoms in the crystalline ZIFs. Combining our experimental results with density functional theory calculations enabled the assignment of all chemical shifts. The crystalline spectra reveal the potential of high field NMR to distinguish between two ZIF polymorphs, ZIF-4 and ZIF-zni, with identical $[Zn(C_3H_3N_2)_2]$ chemical compositions. ^{13}C and ^{15}N CP MAS NMR data obtained for the amorphous ZIFs clearly showed signal broadening upon amorphization, confirming the retention of chemical composition and the structural similarity of amorphous ZIF-4 and ZIF-zni. In the case of amorphous ZIF-8, we present evidence for the partial de-coordination of the 2-methyl imidazole linker.

Introduction

Metal–organic frameworks (MOFs) are three-dimensional polymeric networks consisting of inorganic metal-ion nodes interconnected by organic linkers. The zeolitic imidazolate framework (ZIF) family, a subset of MOFs, are microporous. These frameworks can possess network topologies identical to those of inorganic zeolites, courtesy of the 145° angle subtended at the bridging imidazolate ($C_3H_3N_2^-$, Im) based ligand.[1,2] However, ZIFs are significantly more porous than their inorganic cousins due to the greater interatomic separation of the metal ions, which is beneficial for greenhouse gas capture[3] and drug delivery.[4]

Solid state nuclear magnetic resonance (NMR) is a well-established technique for atomic scale structural characterization.[5] Both NMR and diffraction methods provide structural, dynamic and host–guest interaction information on metal–organic frameworks.[6,7] NMR has previously been used to study organic-sub units in MOFs and their role within the framework, for example in the mixed ligand MIL-53(Al)[8] and the functional groups in multivariant MOF-5.[9] Through NMR studies, information on gas adsorbate location, motion and binding can also be revealed, as studied for the uptake of CO_2 in Mg_2(dobdc) (H_4dobdc = 2,5-dihydroxyterephtalic acid).[10] When the sole use of X-ray techniques is inadequate for resolving new structures, combination with solid state NMR allows for detailed information to be gained on local chemical environments, such as structure elucidation, topology and coordination environments in MIL-110.[11]

ZIF NMR studies have been used to monitor the flexibility of ZIF-4 and ZIF-8 at variable temperatures,[12] whilst combination with powder X-ray diffraction (PXRD) permitted the analysis of packing and topology in crystalline ZIF-8 and $Zn(EtIm)_2$, using a low magnetic field (7–11.7 T).[13] NMR techniques applied to ZIF-8 have been successful in monitoring orientations and movement of benzene within the framework,[14] the self-diffusion of adsorbed gases,[15] and structural changes at low temperatures.[16]

Recent advances in computational methodology have allowed for accurate and efficient prediction of NMR chemical shifts in solids.[17,18] For example, this approach has been used to elucidate the structure of new MOFs, such as $[ZnAlF_5{\cdot}TAZ]$ (TAZ = triazolate ligand, $C_3H_2N_3O_2$).[19] High field 21.1 T ^{67}Zn NMR and computational work on ZIF-8 was able to provide structural information on the Zn environments.[20] A further

[a] *Department of Materials Science and Metallurgy, University of Cambridge, 27 Charles Babbage Road, Cambridge, CB3 0FS, UK. E-mail: akc30@cam.ac.uk*
[b] *Laboratoire de Chimie des Processus Biologiques, CNRS-UMR 8229, Collège de France, 11 Place Marcelin Berthelot, 75005, Paris, France*
[c] *Sorbonne Universités, UPMC Univ Paris 06, CNRS, Collège de France, UMR 7574, Chimie de la Matière Condensée de Paris, Paris, France*
[d] *Department of Chemistry and Stephenson Institute for Renewable Energy, University of Liverpool, Crown Street, Liverpool, L69 7ZD, UK*

† Electronic supplementary information (ESI) available. See DOI: 10.1039/c5cp02552d

example includes the use of high resolution ^{1}H NMR, in conjunction with DFT calculations, which has recently been used to resolve the super cell structure of a new ZIF-8 analogue material, SIM-1.[21]

Temperature,[22] pressure[23] and ball milling[24] have been shown to induce structural collapse for a range of crystalline ZIFs, resulting in a loss of porosity and the formation of amorphous MOFs. In the latter instance, the highly disordered structures formed have been termed a_mZIFs, where the subscript m refers to amorphization induced by ball-milling. Despite work confirming the retention of intra-organic and organic–inorganic bonding, in *a*ZIF materials, many amorphous reaction products are still discarded due to the lack of a facile and fast characterization technique.[25]

This investigation presents high field ^{13}C and ^{15}N CP (cross polarisation) MAS (magic angle spinning) solid-state NMR spectra of several crystalline ZIF structures. The NMR data accurately distinguish between ZIFs that possess different network topologies, identifying all crystallographically independent carbon and nitrogen atoms. Combination of the experimental data with modern computational methods allows for the assignment of ^{13}C and ^{15}N NMR chemical shifts. We also used high field CP MAS NMR to study a range of a_mZIFs, demonstrating the ability of NMR to gain useful structural information on these highly disordered materials.

Methods

Sample preparation and crystallographic details

ZIF-zni ($[Zn(C_3H_3N_2)_2]$) was synthesized according to a previously published procedure,[13] ZIF-8 ($[Zn(C_4H_5N_2)_2]$) was purchased from BASF, and ZIF-4 ($[Zn(C_3H_3N_2)_2]$) was prepared using a modified synthesis protocol, as described in the ESI† (S1). Note that ZIF-8 contains 2-methyl imidazole as the linker, whereas the ZIF-zni and ZIF-4 contain unsubstituted imidazole and are therefore polymorphs. ZIF-zni crystallises in the space group $I4_1cd$ and contains 4 crystallographically independent organic linkers,[26] (a = 23.481 Å, b = 23.481 Å, c = 12.461 Å, V = 6870.464 Å^3). ZIF-4, exists in the orthorhombic space group $Pbca$ (a = 15.402(7) Å, b = 15.459(7) Å, c = 18.408(8) Å, V = 4383(3) Å^3)[23] and also contains 4 independent organic linkers. ZIF-8 (topologically identical to the inorganic zeolite sodalite), crystallises in the isotropic space group $I\bar{4}3m$ (a = 16.9856(16) Å, V = 4900.5(8) Å^3) and contains only 5 crystallographically independent atoms (Fig. 1a).[1]

Solid-state NMR

All solid-state NMR experiments were performed on a 20 T Bruker Avance II solid-state NMR spectrometer equipped with a 3.2 mm HXY triple-resonance MAS probe at $\nu_0(^1\mathrm{H})$ = 850.23 MHz, with the X channel tuned to ^{13}C at $\nu_0(^{13}\mathrm{C})$ = 213.81 MHz and Y channel tuned to ^{15}N at $\nu_0(^{15}\mathrm{N})$ = 86.17 MHz. All experiments were performed under MAS at ν_r = 21 kHz at 26 °C and with a 2 s recycle delay. All ^{1}H pulses and SPINAL-64 heteronuclear decoupling[28] were performed at a radio-frequency (rf) field amplitude of 83 kHz. ^{1}H ^{13}C CP MAS experiments were obtained with contact times of 2 ms and with a ^{13}C rf field of 55 kHz, while the ^{1}H rf field amplitude was ramped to obtain maximum signal at a ^{1}H rf field of approximately 75 kHz. ^{1}H ^{15}N CP MAS experiments were obtained with contact times of 5 ms and with a ^{15}N rf field of 38 kHz, while the ^{1}H rf field amplitude was ramped to obtain maximum signal at a ^{1}H rf field of approximately 57 kHz. Additional ^{13}C CP MAS spectrum of ZIF-4 was obtained on a 9.4 T Bruker Avance III HD solid-state NMR spectrometer equipped with a 4 mm HXY triple-resonance MAS probe (in double-resonance mode) at $\nu_0(^1\mathrm{H})$ = 400.13 MHz and $\nu_0(^{13}\mathrm{C})$ = 100.62 MHz under MAS at ν_r = 21 kHz at room temperature and with a 3 s recycle delay. ^{1}H pulses and SPINAL-64 heteronuclear decoupling[28] were performed at a radio-frequency (rf) field amplitude of 83 kHz. ^{1}H ^{13}C CP MAS experiments were obtained with a contact time of 2 ms and with a ^{13}C rf field of 40 kHz, while the ^{1}H rf field amplitude was ramped to obtain maximum signal at a ^{1}H rf field of approximately 60 kHz. The number of scans for each sample is given in Table S6 (ESI†). ^{13}C and ^{15}N chemical shifts (±0.2 ppm) were externally referenced at room temperature to the CH_3 group of alanine at 20.5 ppm (corresponding to the CH_2 group of adamantane at 29.45 ppm)[29] and the NH_3^+ group of alanine at 52.4 ppm (corresponding to liquid NH_3 at 0 ppm). All samples were packed in air.

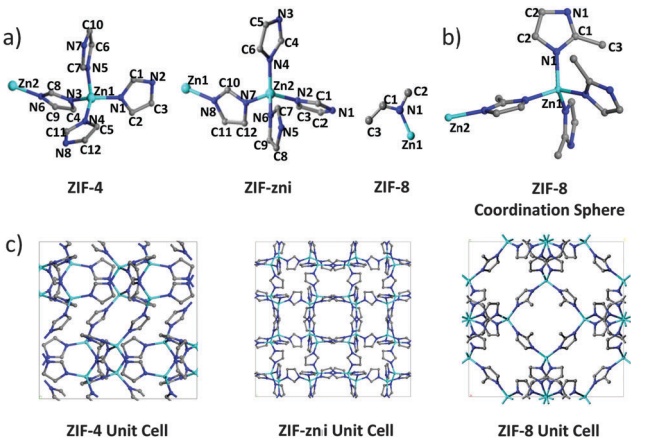

Fig. 1 (a) The asymmetric units of ZIF-4, ZIF-zni and ZIF-8. (b) ZIF-8 coordination sphere generated using the Mercury software.[27] Zn – light blue, N – purple, C – grey. H atoms have been omitted for clarity. (c) The unit cells of the three ZIFs.

Computational methods

All electronic and structural calculations on the ZIFs were performed with the Kohn–Sham DFT framework using periodic boundary conditions. Starting from each experimentally determined crystal structure, both lattice parameters and atomic positions were fully relaxed in space group $P1$ with the semi-local Perdew–Burke–Ernzerhof exchange–correlation functional using D2 dispersion corrections by Grimme *et al.*[30] The Vienna ab initio package (VASP)[31] a planewave code, was employed for these geometry optimizations. A 500 eV plane-wave cutoff was found suitable for the convergence of the systems to within 0.01 eV per atom.

It is important to highlight here the key role of the dispersion interactions in the modelling of ZIFs. It has been shown in a number of computational studies that the long-range dispersion interactions play a key role in the energy landscape of hybrid frameworks, such as the highly flexible MIL-53[32] or the family of ZIFs solids[33] whereby the simple inverse relationship between density and thermodynamic stability is captured. More recently, we have shown how DFT-D calculations may predict the structure-directing influence of functionalized linkers in ZIFs.[34] Also DFT-D calculations are necessary to predict the mechanical properties of the Zn- and LiB-zni.[35]

The first principles NMR calculations were performed within Kohn–Sham DFT using the QUANTUM-ESPRESSO software (available online).[36] The PBE generalized gradient approximation[37] was used and the valence electrons were described by norm conserving pseudopotentials[38] in the Kleinman–Bylander[39] form. The wave functions are expanded on a plane wave basis set with a kinetic energy cut-off of 1088 eV. The integral over the first Brillouin zone are performed using a Monkhorst–Pack $2 \times 2 \times 2$ k-point grid for the charge density and chemical shift tensor calculation. The shielding tensor is computed using the GIPAW[40] approach which permits the reproduction of the results of a fully converged all-electron calculation. The isotropic chemical shift δ_{iso} is defined as $\delta_{iso} = -[\sigma - \sigma^{ref}]$ where σ is the isotropic shielding and σ^{ref} is the isotropic shielding of the same nucleus in a reference system. In the present case, the comparison between the experimental δ_{iso} and calculated σ_{iso} ^{13}C and ^{15}N chemical shift values for carboxylate of α-glycine[41] (δ_{iso} = 176.2 ppm)[42] and for CH_3NO_2[43] (δ_{iso} = 380.2 ppm corresponding to NH_3 at 0 ppm) respectively, allowed to determine σ^{ref} for these nuclei.

Amorphization

Amorphization of the ZIFs was performed by following a published procedure.[24] Typically, 0.2 g of crystalline ZIF material was placed in a stainless steel jar along with an 8 mm stainless steel ball. The jar was oscillated at 20 Hz for various times using a Retsch MM200 mill resulting in an amorphous material.

Results and discussion

Solid-state NMR analysis of crystalline ZIFs

The ^{13}C and ^{15}N CP MAS NMR spectra of the ZIF samples recorded at 20 T are presented in Fig. 2 (Fig. S3 and S4, ESI†). Use of a high field allows observation of all individual carbon and nitrogen atoms in the asymmetric units, which is not possible at lower fields of 7 T.[12] Furthermore, the ^{13}C and ^{15}N spectra for the two polymorphs, ZIF-zni and ZIF-4, are strikingly different, reflecting their very different structures (Fig. 2). Note that the ^{13}C line widths are slightly broader for ZIF-4 than for ZIF-zni, which we ascribe to differences in their crystallinities. The asymmetric unit of ZIF-8 contains 1 N, 1 Zn and 3 C atoms (Fig. 1a). The ^{13}C CP MAS NMR spectrum of ZIF-8 displays 3 peaks (Fig. 2a), as anticipated. The peak at 13.7 ppm is typical

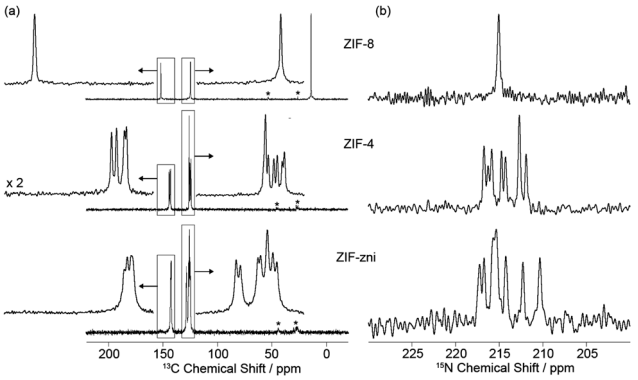

Fig. 2 (a) ^{13}C CP MAS and (b) ^{15}N CP MAS spectra of crystalline ZIFs recorded on a Bruker 20 T Avance II solid-state NMR spectrometer with $\nu_0(^1H)$ = 850.23 MHz, $\nu_0(^{13}C)$ = 213.81 MHz and $\nu_0(^{15}N)$ = 86.17 MHz under MAS at ν_r = 21 kHz and SPINAL-64 ^{1}H decoupling[28] with $\nu_1(^1H)$ = 83 kHz. Further details about the acquisitions parameters are given in Table S6 (ESI†). Spinning sidebands are marked with asterisks. In (a), the left and right inserts show magnified views of the 154–140 ppm and 132–122 ppm regions, respectively.

for a methyl group, whereas the two other peaks, downfield at 124.2 (N*C*C) and 151.2 ppm (N*C*CH_3N) correspond to the carbons within the aromatic ring. As cross-polarised ^{13}C spectra are not quantitative, the intensities of the peaks do not necessarily correspond with the populations of the different sites.[5] The single nitrogen present in the asymmetric unit is recorded at 214.4 ppm in the ^{15}N NMR spectrum and is in agreement with previous reports.[12,13]

The asymmetric unit of ZIF-4 contains 8 N, 12 C and 2 Zn atoms (Fig. 1a). The ^{13}C spectra display two groups of peaks in the region of 120–155 ppm. The 6 peaks at 123.9–125.8 ppm are, to a good approximation, well resolved and correspond to the 8 carbon environments N*C*C (the signal at 125.6 ppm integrating for 3 carbons), labelled C2, C3, C4, C5, C6, C9, C10 and C12 in Fig. 1. The N*C*N carbon signals appear well resolved at 142.5–143.9 ppm for the remaining C1, C7, C8 and C11 (Fig. 1a) carbon environments, showing that the spectrum can be fully resolved for all 12 carbon environments. The 7 nitrogen atom signals are well resolved in the ^{15}N spectrum, the signal at 212.0 ppm corresponding to 2 nitrogens. The peak at 215.6 ppm in the ^{15}N spectrum is slightly lower in intensity and is broader with a full width half maximum (FWHM) of 32 Hz *vs.* 22–24 Hz for the other ^{15}N signals. Full assignment of the ^{15}N ZIF-4 NMR spectrum is not practical without recourse to computational work.

ZIF-zni possesses 8 N, 12 C and 2 Zn atoms in the asymmetric unit (Fig. 1a) and is chemically identical to ZIF-4 yet adopting different network connectivity, as previously mentioned. Similarly to ZIF-4, the ^{13}C ZIF-zni spectrum contains two sets of peaks in the range of 120–155 ppm belonging to the imidazolate-based carbon atoms. The 4 peaks at 142–142.7 ppm represent the N*C*N environments, C1, C4, C7 and C10, and are partially resolved. The 8 N*C*C environments appear in the spectrum in the range of 124.5–128.3 ppm, where the peak at 125.4 represents 2 carbons, and are assigned to C2, C3, C5, C6 C8, C9, C11 and

C12. It is, however, apparent in the spectra of ZIF-zni that there are two outlying peaks within the N*C*C set, which we later show on the basis of the computational calculations (*vide infra*), are assigned to C9 at 128.3 and C12 at 127.8 ppm. The ^{15}N spectrum displays 8 partially resolved nitrogen environments, which again can be assigned in combination with DFT calculations.

The highly resolved NMR spectra of ZIF-4 and ZIF-zni are in agreement with the presence of 4 crystallographically independent imidazolate ligands, as previously determined by single crystal diffraction.[1] More importantly, this demonstrates that different ^{13}C and ^{15}N NMR spectra are obtained for the two ZIF polymorphs at high field (20 T), corresponding to subtle differences in the coordination of the tetrahedral Zn^{2+} ions. These findings complement the information that is obtained from neutron and X-ray diffraction data.[22]

Computational results

In order to make further progress with NMR assignments, DFT methods were used to calculate NMR shifts for the three crystalline frameworks. Assignments of the experimental chemical shifts were carried out according to the DFT calculations. On this basis, the two outliers in the ZIF-zni ^{13}C spectra could be assigned (ESI,† Table S2). It should be noted that ^{13}C and ^{15}N NMR parameters were calculated for all carbon and nitrogen positions obtained after dispersion-corrected DFT-D2 full relaxation calculations of the structures, taken from our previous computational study of ZIF energy landscapes.[33] The calculations were performed in space group *P*1, and the values obtained for crystallographically equivalent atoms were averaged to allow for direct comparison with the experimental crystal structures. An attribution of the different sites could then be proposed by comparing the isotropic experimental and calculated chemical shift values, the results (Fig. 3 and ESI,† Tables S1–S3) showing excellent agreement.

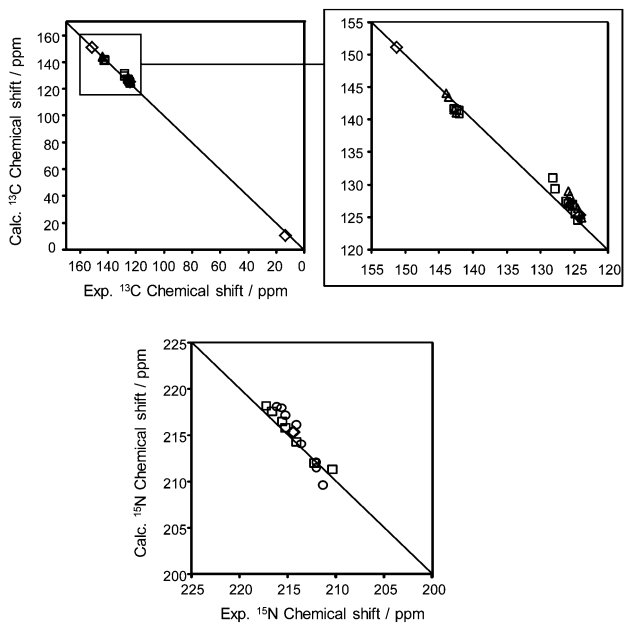

Fig. 3 Combined plots of the ^{13}C and ^{15}N calculated isotropic chemical shifts δ_{iso} *versus* the experimental values of ZIF-8 (open diamonds), ZIF-zni (open squares) and ZIF-4 (open circles) structures. Insert shows a magnified view of the 155–120 ppm region. The lines are given as a guide to the eye and correspond to perfect fits between experiments and calculations.

Solid-state NMR analysis of amorphous ZIFs

All amorphous ZIFs were prepared by ball-milling following a known procedure.[24] Previous X-ray total scattering measurements of amorphous ZIF were unable to distinguish between samples derived from different crystalline precursors.[44] Our NMR results for a_mZIF-4 and a_mZIF-zni confirm that the imidazole linker remains intact in the amorphous products, but also shows that their ^{13}C and ^{15}N spectra are indistinguishable (Fig. 4 and ESI,† Table S5); two broad peaks at 126 (N*C*C) and 143 ppm (N*C*N) are observed in the ^{13}C spectra while a single broad signal centred at 215 ppm is detected in the ^{15}N spectra. The coalescence of peaks, post amorphization, indicates not only a loss of distinct environments, but also the averaging of the previously distinct chemical environments. Note that there is no significant difference between the ^{1}H T_1 relaxation times of crystalline and amorphized ZIF-4.

The three different ^{13}C signals observed for crystalline ZIF-8 (Fig. 2a) are retained upon amorphization, though they broaden significantly, as do those in the ^{15}N spectrum. Two additional signals at 148 and 118 ppm are observed in the ^{13}C spectrum of a_mZIF-8. Given the absence of such signals in crystalline ZIF-8, we propose that ligand de-coordination arising from the breaking of Zn-2-methylimidazolate bonds results in free 2-methylimidazolate which could not be detected in the previous X-ray studies. The ^{13}C NMR spectrum of 2-methylimidazole[45] contains peaks at 144.8, 125.4, 115.6 and 13.8 ppm; those at 125.4 and 13.4 ppm are obscured by a_mZIF-8 itself (Table S5, ESI†), but the remaining two match well with our additional peaks at 148 and 118 ppm. It is

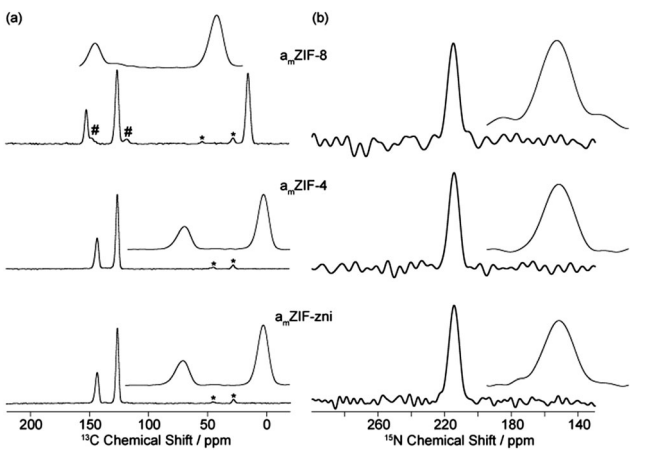

Fig. 4 (a) ^{13}C and (b) ^{15}N CP MAS spectra of amorphous ZIFs recorded on a Bruker 20 T Avance II solid-state NMR spectrometer with $\nu_0(^1H)$ = 850.23 MHz and $\nu_0(^{13}C)$ = 213.81 MHz under MAS at ν_{rot} = 21 kHz and SPINAL-64 ^{1}H decoupling[28] with $\nu_1(^1H)$ = 83 kHz. Further details about the acquisitions parameters are given in Table S6 (ESI†). Spinning sidebands are marked with asterisks and the additional peaks due to free ligand in the case of a_mZIF-8 are indicated by # symbols. In (a) and (b), inserts show a magnified view of the 155–120 ppm and 230–200 ppm region, respectively.

also consistent with previous work on the ball milling of zeolites, which involves breaking Si–O–Si external linkages and formation of quasicrystalline particles.[46]

Conclusions

^{13}C and ^{15}N MAS NMR spectra of three crystalline ZIFs were obtained and the peaks were assigned using DFT chemical shift calculations. All crystallographically independent carbon and nitrogen atoms were identified. The chemically identical but topologically different ZIF-4 and ZIF-zni were distinguishable through NMR analysis. The ^{13}C and ^{15}N spectra obtained for the chemically equivalent amorphous ZIFs confirm their structural similarity and are in agreement with prior PDF results suggesting that a_mZIF-4 and a_mZIF-zni phases are identical. a_mZIF-8, however, shows evidence of ligand de-coordination that was not detected in previous X-ray studies. NMR is a promising technique for gaining structural insight into amorphous MOFs, before recourse to more time-consuming structural analysis *via* total X-ray scattering measurements.

Conflict of interest

The authors declare no competing financial interests.

Funding sources

We acknowledge funding from the EPSRC (EB), Trinity Hall (TDB), the University of Liverpool (FB) and the ERC (AKC).

Acknowledgements

The UK 850 MHz solid-state NMR Facility used in part of this research was funded by EPSRC and BBSRC, as well as the University of Warwick including partial funding through Birmingham Science City Advanced Materials Projects 1 and 2 supported by Advantage West Midlands (AWM) and the European Regional Development Fund (ERDF). NMR calculations were performed on the IDRIS supercomputer center of the CNRS (Project 091461). CMD acknowledges support from Fondation de l'Orangerie for individual Philanthropy and its donors and thanks the ANR project HOPFAME (ANR-13-420 BS07-0002-01).

Notes and references

1 K. S. Park, Z. Ni, A. P. Côté, J. Y. Choi, R. Huang, F. J. Uribe-Romo, H. K. Chae, M. O'Keeffe and O. M. Yaghi, *Proc. Natl. Acad. Sci. U. S. A.*, 2006, **103**, 10186–10191.
2 Y.-Q. Tian, Y.-M. Zhao, Z.-X. Chen, G.-N. Zhang, L.-H. Weng and D.-Y. Zhao, *Chem. – Eur. J.*, 2007, **13**, 4146–4154.
3 A. Phan, C. J. Doonan, F. J. Uribe-Romo, C. B. Knobler, M. O'Keeffe and O. M. Yaghi, *Acc. Chem. Res.*, 2010, **43**, 58–67.
4 N. Liédana, A. Galve, C. Rubio, C. Téllez and J. Coronas, *ACS Appl. Mater. Interfaces*, 2012, **4**, 5016–5021.
5 D. D. Laws, H.-M. L. Bitter and A. Jerschow, *Angew. Chem., Int. Ed.*, 2002, **41**, 3096–3129.
6 A. Sutrisno and Y. Huang, *Solid State Nucl. Magn. Reson.*, 2013, **49–50**, 1–11.
7 S. E. Ashbrook, D. M. Dawson and V. R. Seymour, *Phys. Chem. Chem. Phys.*, 2014, **16**, 8223–8242.
8 Y. Jiang, J. Huang, S. Marx, W. Kleist, M. Hunger and A. Baiker, *J. Phys. Chem. Lett.*, 2010, **1**, 2886–2890.
9 X. Kong, H. Deng, F. Yan, J. Kim, J. A. Swisher, B. Smit, O. M. Yaghi and J. A. Reimer, *Science*, 2013, **341**, 882–885.
10 X. Kong, E. Scott, W. Ding, J. A. Mason, J. R. Long and J. A. Reimer, *J. Am. Chem. Soc.*, 2012, **134**, 14341–14344.
11 C. Volkringer, D. Popov, T. Loiseau, N. Guillou, G. Ferey, M. Haouas, F. Taulelle, C. Mellot-Draznieks, M. Burghammer and C. Riekel, *Nat. Mater.*, 2007, **6**, 760–764.
12 W. Morris, C. J. Stevens, R. E. Taylor, C. Dybowski, O. M. Yaghi and M. A. Garcia-Garibay, *J. Phys. Chem. C*, 2012, **116**, 13307–13312.
13 P. J. Beldon, L. Fábián, R. S. Stein, A. Thirumurugan, A. K. Cheetham and T. Friščić, *Angew. Chem., Int. Ed.*, 2010, **49**, 9640–9643.
14 D. I. Kolokolov, L. Diestel, J. Caro, D. Freude and A. G. Stepanov, *J. Phys. Chem. C*, 2014, **118**, 12873–12879.
15 A.-K. Pusch, T. Splith, L. Moschkowitz, S. Karmakar, R. Biniwale, M. Sant, G. Suffritti, P. Demontis, J. Cravillon, E. Pantatosaki and F. Stallmach, *Adsorption*, 2012, **18**, 359–366.
16 M.-A. Springuel-Huet, A. Nossov, F. Guenneau and A. Gedeon, *Chem. Commun.*, 2013, **49**, 7403–7405.
17 C. Bonhomme, C. Gervais, F. Babonneau, C. Coelho, F. Pourpoint, T. Azaïs, S. E. Ashbrook, J. M. Griffin, J. R. Yates, F. Mauri and C. J. Pickard, *Chem. Rev.*, 2012, **112**, 5733–5779.
18 S. E. Ashbrook and D. M. Dawson, *Acc. Chem. Res.*, 2013, **46**, 1964–1974.
19 A. Cadiau, C. Martineau, M. Leblanc, V. Maisonneuve, A. Hemon-Ribaud, F. Taulelle and K. Adil, *J. Mater. Chem.*, 2011, **21**, 3949–3951.
20 A. Sutrisno, V. V. Terskikh, Q. Shi, Z. Song, J. Dong, S. Y. Ding, W. Wang, B. R. Provost, T. D. Daff, T. K. Woo and Y. Huang, *Chem. – Eur. J.*, 2012, **18**, 12251–12259.
21 M. Baias, A. Lesage, S. Aguado, J. Canivet, V. Moizan-Basle, N. Audebrand, D. Farrusseng and L. Emsley, *Angew. Chem., Int. Ed.*, 2015, **54**, 5971–5976.
22 T. D. Bennett, A. L. Goodwin, M. T. Dove, D. A. Keen, M. G. Tucker, E. R. Barney, A. K. Soper, E. G. Bithell, J.-C. Tan and A. K. Cheetham, *Phys. Rev. Lett.*, 2010, **104**, 115503.
23 T. D. Bennett, P. Simoncic, S. A. Moggach, F. Gozzo, P. Macchi, D. A. Keen, J.-C. Tan and A. K. Cheetham, *Chem. Commun.*, 2011, **47**, 7983–7985.
24 T. D. Bennett, S. Cao, J. C. Tan, D. A. Keen, E. G. Bithell, P. J. Beldon, T. Friščić and A. K. Cheetham, *J. Am. Chem. Soc.*, 2011, **133**, 14546–14549.

25 D. G. H. D. Lau, M. R. Hill, B. W. Muir, S. A. Furman and D. F. Kennedy, *Comb. Chem. High Throughput Screening*, 2011, **14**, 28–35.
26 T. Wu, X. Bu, J. Zhang and P. Feng, *Chem. Mater.*, 2008, **20**, 7377–7382.
27 C. F. Macrae, I. J. Bruno, J. A. Chisholm, P. R. Edgington, P. McCabe, E. Pidcock, L. Rodriguez-Monge, R. Taylor, J. van de Streek and P. A. Wood, *J. Appl. Crystallogr.*, 2008, **41**, 466–470.
28 B. M. Fung, A. K. Khitrin and K. Ermolaev, *J. Magn. Reson.*, 2000, **142**, 97–101.
29 C. R. Morcombe and K. W. Zilm, *J. Magn. Reson.*, 2003, **162**, 479–486.
30 S. Grimme, *J. Comput. Chem.*, 2006, **27**, 1787–1799.
31 G. Kresse and J. Furthmüller, *Phys. Rev. B: Condens. Matter Mater. Phys.*, 1996, **54**, 11169–11186.
32 A. M. Walker, B. Civalleri, B. Slater, C. Mellot-Draznieks, F. Corà, C. M. Zicovich-Wilson, G. Román-Pérez, J. M. Soler and J. D. Gale, *Angew. Chem., Int. Ed.*, 2010, **49**, 7501–7503.
33 R. Galvelis, B. Slater, A. K. Cheetham and C. Mellot-Draznieks, *CrystEngComm*, 2012, **14**, 374–378.
34 R. Galvelis, B. Slater, R. Chaudret, B. Creton, C. Nieto-Draghi and C. Mellot-Draznieks, *CrystEngComm*, 2013, **15**, 9603–9612.
35 T. D. Bennett, J.-C. Tan, S. A. Moggach, R. Galvelis, C. Mellot-Draznieks, B. A. Reisner, A. Thirumurugan, D. R. Allan and A. K. Cheetham, *Chem. – Eur. J.*, 2010, **16**, 10684–10690.
36 P. Giannozzi, N. Bonini, S. Baroni, M. Calandra, R. Car, C. Cavazzoni, D. Ceresoli, G. L. Chiarotti, M. Cococcioni, I. Dabo, A. Dal Corso, S. Fabris, G. Fratesi, S. de Gironcoli, R. Gebauer, U. Gerstmann, C. Gougoussis, A. Kokalj, M. Lazzeri, L. Martin-Samos, N. Marzari, F. Mauri, R. Mazzarello, S. Paolini, A. Pasquarello, L. Paulatto and C. Sbraccia, *J. Phys.: Condens. Matter*, 2009, **21**, 395502.
37 J. P. Perdew, K. Burke and M. Ernzerhof, *Phys. Rev. Lett.*, 1996, **77**, 3865–3868.
38 N. Troullier and J. L. Martins, *Phys. Rev. B: Condens. Matter Mater. Phys.*, 1991, **43**, 1993–2006.
39 L. Kleinman and D. M. Bylander, *Phys. Rev. Lett.*, 1982, **48**, 1425–1428.
40 C. J. Pickard and F. Mauri, *Phys. Rev. B: Condens. Matter Mater. Phys.*, 2001, **63**, 245101.
41 P.-G. Jonsson and A. Kvick, *Acta Crystallogr., Sect. B: Struct. Crystallogr. Cryst. Chem.*, 1972, **28**, 1827–1833.
42 C. Gervais, R. Dupree, K. J. Pike, C. Bonhomme, M. Profeta, C. J. Pickard and F. Mauri, *J. Phys. Chem. A*, 2005, **109**, 6960–6969.
43 S. F. Trevino, E. Prince and C. R. Hubbard, *J. Chem. Phys.*, 1980, **73**, 2996–3000.
44 T. D. Bennett, D. A. Keen, J.-C. Tan, E. R. Barney, A. L. Goodwin and A. K. Cheetham, *Angew. Chem., Int. Ed.*, 2011, **50**, 3067–3071.
45 C. López, R. Claramunt, M. Á. García and J. Elguero, *Cent. Eur. J. Chem.*, 2004, **2**, 660–671.
46 C. Kosanović, J. Bronić, B. Subotić, I. Smit, M. Stubičar, A. Tonejc and T. Yamamoto, *Zeolites*, 1993, **13**, 261–268.

